Metrology for III-V Optosemiconductors

Hans Baumgartner

Metrology for III-V Optosemiconductors

Hans Baumgartner

A doctoral dissertation completed for the degree of Doctor of Science (Technology) to be defended, with the permission of the Aalto University School of Electrical Engineering, at a public examination held at the lecture hall TU1 of the school on 9th June 2017 at 12.

Aalto University
School of Electrical Engineering
Department of Signal Processing and Acoustics
Metrology Research Institute

Supervising professor
Prof. Erkki Ikonen

Thesis advisor
Doc. Petri Kärhä

Preliminary examiners
Prof. Mircea Guina, Tampere University of Technology, Finland
Prof. Grega Bizjak, University of Ljubljana, Slovenia

Opponent
Prof. Peter Hanselaer, University of Leuven, Ghent, Belgium

NORDIC ECOLABEL

441   697
Printed matter

Abstract

Light-emitting diodes (LEDs) are III-V compound semiconductors manufactured by combining elements from group III (such as Al, Ga, and In) with elements from group V (such as N, P, As), forming compounds like GaN, GaInAs, and AlInP. High-power white LEDs are manufactured by coating a blue or an ultraviolet (UV) LED with phosphor, absorbing part of the blue/UV photons and emitting them at higher wavelengths. High-power LEDs are typically packaged to form an optosemiconductor device with a power rating between 1 and 5 W.

In addition to light-emitting devices, III-V optosemiconductor devices can be utilized as photon absorbing, multi-junction solar cells. The materials and manufacturing processes for LEDs and III-V solar cells are the same, making their electrical and optical properties similar. In this thesis, measurement setups and novel analysis methods have been developed for luminous efficacy, lifetime, and band gap energy of LEDs and multi-junction solar cells manufactured using III-V materials.

The lifetime of high-power LEDs was studied by aging different types of LED lamps at room temperature and at elevated temperatures of 45 °C and 60 °C. The aging was measured as the change of luminous flux over time. The aging accelerated on the average by factors of 1.35 and 2.36 when aging the LEDs at the elevated temperatures. The lifetime of high quality LEDs was shown to be more than 50 000 hours and projected with a new method to exceed 100 000 hours.

Despite the high efficiency of LEDs, most of the consumed electrical power is still wasted in the form of heat, weakening the lifetime and optical characteristics of the optosemiconductor devices. To study the effect of temperature on the optical characteristics of high-power LEDs and multi-junction solar cells, a temperature controller based on liquid cooling and resistive heating was designed and built.

A novel model for the emission spectrum of an LED was developed to determine the band gap energy of the device under tests. The method was shown to work in determining the alloy composition of III-V LEDs. The method was tested and utilized to determine the band gap energies of III-V multi-junction solar cells as well. The developed method can be used to determine temperature-invariant band gap characteristics of all III-V optosemiconductor devices.

A! Aalto-yliopisto

Tiivistelmä

Ledejä käytettiin pitkään pääasiassa elektronisten laitteiden merkkivaloina. Suuritehoisen valkoisen ledin kehitys 2000-luvun alussa laajensi ledien käytön myös yleisvalaistukseen ja nykyään suurin osa yleisvalaistuksesta toteutetaan ledien avulla.

Ledit ovat puolijohdekomponentteja, jotka on valmistettu käyttäen materiaaleja alkuaineryhmistä III ja V, muodostaen yhdisteitä kuten GaN, GaInAs ja AlInP. Valaistuksessa käytetyt valkoiset ledit ovat tyypillisesti fosforilla päällystettyjä ledejä, jotka emittoivat sinistä tai ultraviolettivaloa. Ledin päällä oleva fosfori absorboi ledistä tulevan valon ja emittoi sen laajalla aallonpituusalueella, muodostaen valkoista valoa. Suuritehoiset ledit on tavallisesti pakattu komponenteiksi, joiden sähköteho on 1-5 W.

Ledien lisäksi, III-V alkuaineesta valmistettuja puolijohdekomponentteja voidaan käyttää pienissä ja tehokkaissa monikerrosaurinkokennoissa. Koska sekä ledeissä, että aurinkokennoissa käytetyt materiaalit ja valmistustekniikka ovat samat, myös sähköiset ja optiset ominaisuudet ovat yhtenevät. Väitöskirjassa on kehitetty uusia mittalaitteistoja sekä analyysimetodeja III-V materiaaleista valmistettujen ledien ja monikerrosaurinkokennojen valotehokkuuden, elinajan ja energiaraon määritykseen.

Suuritehoisten ledien elinaikaa tutkittiin ikäännyttämällä erityyppisiä led-lamppuja huoneenlämpötilassa sekä korotetuissa, 45 ja 60 asteen lämpötiloissa. Korotetuissa lämpötiloissa suoritettu ikäännyttäminen kiihdytti ikääntymistä keskimäärin kertoimilla 1.35 ja 2.36, verrattuna huoneenlämpötilassa suoritettuun ikäännyttämiseen. Hyvälaatuisten ledien eliniäksi voitiin osoittaa yli 50 000 tuntia, ennustetun elinian ollessa yli 100 000 tuntia.

Ledien korkeasta hyötysuhteesta huolimatta suurin osa ledien käyttämästä sähkötehosta muuttuu lämmöksi, heikentäen puolijohdekomponenttien elinikää ja optisia ominaisuuksia. Väitöskirjassa kehitettiin nesteen avulla tapahtuvaan jäähdytykseen ja resistiiviseen lämmitykseen perustuva lämpötilasäädin, jonka avulla suuritehoisten puolijohdekomponenttien lämpötilaa voitiin nopeasti ja tehokkaasti säätää. Laitteiston avulla tutkittiin III-V ryhmien alkuainesta valmistettujen puolijohteiden energiaraon lämpötilariippuvuutta.

Työssä kehitettiin uusi malli ledin emissiospektrin kuvaamiseen. Mallin avulla pystyttiin määrittämään puolijohdeyhdisteen suhteellinen koostumus. Kehitetyn mallin todettiin toimivan myös monikerrosaurinkokennojen energiarakojen määrityksessä.

Contents

List of Abbreviations and Symbols

Abbreviations

Al	Aluminum
AlGaAs	Aluminum gallium arsenide
As	Arsenic
AsH_3	Arsine
CCD	Charge-Coupled Device
CCT	Correlated Color Temperature
Ga	Gallium
GaAs	Gallium arsenide
GaN	Gallium nitride
Ge	Germanium
H_2	Hydrogen (gas)
H^-	Hydride
IC	Integrated Circuit
In	Indium
InGaAlP	Aluminum gallium indium phosphide
LED	Light Emitting Diode
LNE	Laboratoire National de metrologie et d'Essais
MJSC	Multi-Junction Solar Cell

MOCVD	Metalorganic Chemical Vapor Deposition
MOVPE	Metalorganic Vapor Phase Epitaxy
MRI	Metrology Research Institute
N_2	Nitrogen (gas)
P	Phosphorus
PH_3	Phosphine
TMAl	TriMethylAluminum
TMGa	TriMethylGallium
TMIn	TriMethylIndium
UV	UltraViolet

Symbols

A	pre-exponential factor
a	fitting parameter
B	initial constant for exponential luminous flux decay
b	fitting parameter
c	speed of light
E	energy of a photon
E_a	activation energy
E_B	intersection energy
h	Planck constant
K_m	maximum luminous efficacy of photopic vision
k_B	Boltzmann constant
p	band gap shift parameter
q	peak energy shift parameter
$R_{r\lambda}$	spectral responsivity of a trap detector
$R_{s\lambda}$	spectral responsivity of a solar cell sample
T	temperature
T_i	temperature
t	time
$V(\lambda)$	photopic spectral luminous efficiency
$Y_{s\lambda}$	output current of the solar cell sample

$Y_{r\lambda}$	output current of the reference detector
α_a	absorption coefficient
α_i	decay rate at temperature T_i
α	decay rate
$\Phi(t)$	luminous flux at time t
Φ_e	spectrum
Φ_v	luminous flux
λ	wavelength
ν	frequency

List of Publications

This doctoral dissertation consists of an overview and the following publications which are referred to in the text by their Roman numerals.

I   H. Baumgartner, A. Vaskuri, P. Kärhä, and E. Ikonen, "A temperature controller for high power light emitting diodes based on resistive heating and liquid cooling," App. Therm. Eng. **71**, 317-323 (2014).

II   H. Baumgartner, D. Renoux, P. Kärhä, T. Poikonen, T. Pulli, and E. Ikonen, "Natural and accelerated aging of LED lamps," Lighting Res. Technol. **48**, 930-942 (2016).

III   H. Baumgartner, A. Vaskuri, P. Kärhä, and E. Ikonen, "Temperature invariant energy value in LED spectra," Appl. Phys. Lett. **23**, 231103 (2016).

IV   H. Baumgartner, B. Oksanen, P. Kärhä, and E. Ikonen, "Optical characterization of III-V solar cells for temperature independent band gap features," Submitted.

Author's Contribution

Publication I: "A temperature controller for high power light emitting diodes based on resistive heating and liquid cooling"

The author designed and built the mechanics and electronics for the temperature controlled LED measurement setup. Thermal modeling and simulation of the heat transfer system was carried out by the author.

Publication II: "Natural and accelerated aging of LED lamps"

The author implemented the setup for natural aging of the selected LED lamps and carried out the regular optical and electrical measurements. The data analysis and LED lifetime projection was carried out by the author.

Publication III: "Temperature invariant energy value in LED spectra"

The author performed most of the optical measurements of the LEDs at different temperatures. The author noted the specific feature of relative spectra intersecting at a unique point. The analysis of the results and development of the novel spectral model for an LED emission spectrum were carried out by the author.

Publication IV: "Optical characterization of III-V solar cells for temperature independent band gap features"

The author took part in the sample manufacturing process by defining the mechanical dimensions and electrical contacting methods of the solar cell samples. The author performed the emission spectrum measurements and the data analysis.

The author wrote the first versions of all manuscripts and revised the articles on the basis of comments by co-authors and referees.

1. Introduction

1.1 Background

Lighting has been estimated to account for 20-40% of the total energy consumption in buildings [1]. Solid-state lighting based on light-emitting diodes (LEDs) offers both excellent energy efficiency and long product lifetimes. Penetration of LED based lighting solutions has been estimated to reduce the household lighting energy consumption by more than 70% [2]. The energy saving potential for outdoor lighting, when replacing high pressure sodium lamps with LED luminaires is estimated to be 66% [3]. European Union started to phase out incandescent light bulbs in 2009 and banned their sale for residential use in 2012 [4]. Because of the phasing out of incandescent light sources, the LED penetration of the global lighting market has been estimated to surpass 60% by 2020 [5].

LEDs are III-V compound semiconductors manufactured by combining group III elements (typically Al, Ga, In) with group V elements (typically N, P, As) [6-8]. The LEDs used in lighting applications are high power LEDs with a typical electrical power rating between 1 and 5 W [9]. Despite the high efficiency of LEDs compared to incandescence based light sources, most of the electricity consumed is still wasted in the form of heat [9]. The characteristics, such as lifetime, band gap energy, and intensity of the emitted light of an LED are highly temperature dependent. Without a proper heat dissipation system, the temperature of the LED will increase and even destroy the device.

In addition to a light-emitting device, semiconductor devices manufactured using semiconductor materials from element groups III-V can absorb photons [8]. In solar cell applications where high efficiency, small size, and light weight are required, III-V solar cells can be utilized. Due to the complex manufacturing process and high price of III-V solar cells, their use has historically been limited to space applications only. However, in recent years the potential of efficient III-

V solar cell technologies has been proven in terrestrial concentrated photovoltaics installations and energy harvesting applications for devices implementing internet of things as well [10, 11].

The lifetime of an LED can be even 100 000 hours. Due to the high reliability of LEDs, they are not likely to fail under traditional or accelerated life tests, thus the real lifetime of an LED is difficult to estimate [12]. One method to project the lifetime of an LED is to measure the output intensity during aging and extrapolate the measurement data. However, this kind of natural aging is time consuming, thus accelerated aging using elevated temperatures and extrapolating the accelerated aging data has been suggested.

As the optical characteristics of III-V optosemiconductors are highly temperature dependent, determining parameters such as output intensity, band gap energy and absorption spectrum are valid only for the temperature they were measured at. Semiconductor devices are typically mounted on a heat dissipation system and the temperature of the semiconductor p-n junction cannot be measured. When using III-V optosemiconductors in metrological applications the junction temperature is a critical parameter and needs to be stabilized [13-15].

1.2 Content of the thesis

High power light-emitting diodes and new types of high efficiency solar cells are both based on optosemiconductor materials from element groups III and V. In this thesis, I have developed novel characterization methods and measurement facilities for III-V optosemiconductors. Many of the measured samples in this thesis are custom manufactured for scientific purposes, but commercial high power LEDs are studied as well. The change of optical properties of high power LEDs during natural and accelerated aging is studied with regular measurements during 50 000 hours. To characterize III-V optosemiconductors for their optical properties, a new method based on a temperature-invariant intersection energy is demonstrated, which can provide information on the semiconductor band gap energy.

Chapter 2 explains background information about the manufacturing process and basic optical properties of high power LEDs and multi-junction solar cells. Chapter 3 focuses on the measurement technologies and facilities used in this thesis to carry out the optical characterization measurements. After the measurement techniques and facilities, the effect of temperature on the optical prop-

erties and lifetime of LEDs is briefly analyzed. The novel band gap characterization method is presented at the end of chapter 3. The conclusions and summary of the results and findings of this thesis are presented in chapter 4.

1.3 Scientific contribution

The thesis contains the following new scientific results:

1. To study the temperature dependence of the optical characteristics of high power LEDs, a temperature stabilizing system providing cooling and heating power of hundreds of watts is required. A temperature controller for high power LEDs based on resistive heating and liquid cooling was build. The cooling based on liquid flow avoids the use of massive heat sinks for the heat dissipation making the device compact and easy to align. The efficiency of commercial Peltier element based temperature controllers is poor and they require an efficient and big heat dissipation assembly. The new temperature stabilization system designed in publication I is powerful and fast, and the heat sink is small making the alignment of the LED attached to the heat sink easy.

2. LEDs are nowadays widely used in lighting applications and the predicted lifetime of an LED can be even more than 10 years. To study the real lifetime of an LED, waiting such a long period of time is practically not possible. In publication II, the lifetime of high power LEDs used for lighting purposes was studied using commercial LED lamps. A lifetime projection model, based on elevated temperatures to accelerate the heating and using aging data collected during a much shorter time period than the predicted lifetime of >10 years, was developed and tested.

3. In publication III, an enhanced model for the LED emission spectra was developed. It was shown that the relative emission spectra, measured at different temperatures, intersect at a unique energy value. This temperature-invariant energy can be found from all LEDs manufactured using semiconductor materials from element groups III-V. The new model and the temperature-invariant energy value can be utilized in determining the alloy composition of the optosemiconductor device. A physical interpretation was given to the temperature-invariant intersection.

4. In addition to LEDs, optosemiconductor alloys containing elements form groups III and V can also be used to manufacture energy efficient multi-junction solar cells (MJSCs). In publication IV, custom made III-V solar cells were studied for their emission and absorption spectral characteristics. The enhanced emission spectrum model, developed in publication III, was utilized to characterize the optical properties of the new type of solar cells. The reciprocity of the emission and absorption spectra was analyzed and the band gaps were determined from both the emission and the absorption spectra. A novel method to characterize the band gap energy of multi-junction solar cells, based on the emission spectra, was developed. The novel method is capable of separating the band gaps of the different layers of multi-junction solar cell devices.

2. III-V semiconductors

Semiconductors are materials with variable electrical characteristics. The electrical properties of a semiconductor, such as band gap energy, conductivity, and sensitivity to heat or mechanical deformation can be manipulated by addition of impurities, known as doping. Silicon is the most widely used material in electronics industry to build semiconductor devices such as transistors, diodes, and integrated circuits (ICs). However, due to the indirect band gap, silicon cannot emit much light [16].

To manufacture an optosemiconductor device, a compound semiconductor is required. Compound semiconductors are devices composed of elements from at least two different groups. Typically, the materials used in optosemiconductors are from groups 13 and 15, or as using the old notation, from groups III and V [17]. Elements used for commercial optosemiconductor compounds are usually aluminum, gallium, and indium from group III and nitrogen, phosphorus, and arsenic from group V.

High power light emitting diodes and multi-junction solar cells are manufactured using compounds of elements from groups III-V. Due to the flexibility of choice of materials, the band gap of the device can be adjusted and the spectral shapes of the emission and absorption spectra varied. The fabrication processes for LEDs and solar cells based on III-V semiconductors are similar. This chapter explains the principles of the manufacturing process and the main optical characteristics of III-V optosemiconductor devices.

2.1   Manufacturing process

III-V semiconductor compounds can be manufactured using techniques such as molecular beam epitaxy, metalorganic chemical vapor deposition (MOCVD) or pulsed laser deposition [18]. One of the most used methods is MOCVD, also known as metalorganic vapor phase epitaxy (MOVPE) [19]. The term metalorganic or organometallic refers to chemical compounds containing at least one

atom of carbon and one atom of metal. The growth of the semiconductor on the substrate is epitaxial, from Greek meaning "arrangement on" [20]. In epitaxy, the crystalline semiconductor layers are grown on the substrate in such a way that the orientation of the grown crystalline layer has a well-defined orientation with respect to the layer beneath.

In epitaxial growth, the lattice constants of the substrate and the layers to be grown need to be identical or closely matched. Because any residual atoms between the layers prevent epitaxy, the reactors require extreme cleanliness and the highest purity chemicals [19].

The simplest case of epitaxy is homoepitaxy, where the substrate and the film to be grown are of the same material, for example silicon on silicon. However, in the case of LEDs and multi-junction solar cells, heteroepitaxy is used, where the materials of the substrate and the different layers are dissimilar. In heteroepitaxy, the lattice constants of the different layers need to be matched. Figure 1 demonstrates the influence of dissimilar lattice constants to the layer structure.
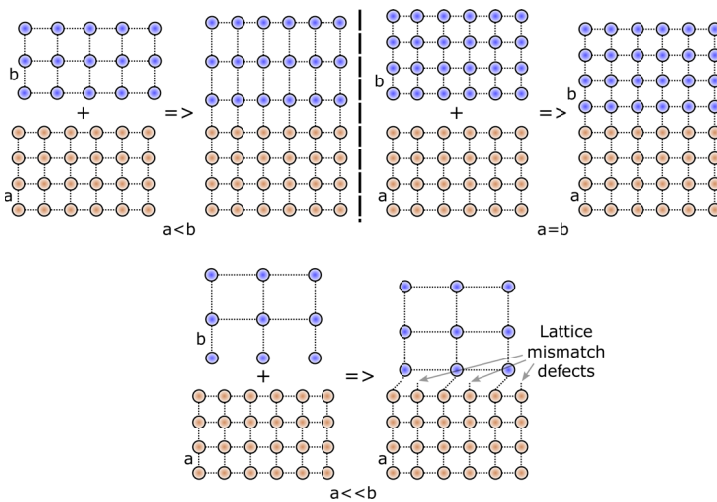
Figure 1: Lattice constants (a and b) of the different layers have to be similar to prevent lattice mismatch defects.

For example, GaAs can be grown on a Ge substrate, because the lattice constants of GaAs and Ge differ less than 0.1%. As seen in Figure 1, if the lattice structures of the different layers do not match, strains are introduced into the layers. If the lattice constants are dissimilar and the thickness of the deposited layer is higher than the critical thickness of the material, the deposited layer cannot stretch or squeeze anymore, inducing defects into the material. Whether the defective material is usable or not, depends on the density and location of the defects. [19, 21]

MOCVD process involves a chemical pyrolysis reaction of vapor phase compounds at high temperatures, typically at the temperature range 600 to 800 ºC [22]. The technology is widely used in both research and volume production of optosemiconductor devices [23]. MOCVD system consists of two main components, the reactor gas delivery system, and the reaction chamber. In addition, due to the toxic gases used and high process temperature, a reactor safety infrastructure is needed.

The reaction gases are delivered to the process chamber through a gas delivery system comprising of different gas sources, alkyl sources, valves, and flow controllers. Figure 2 shows the schematic diagram of a typical gas delivery system.
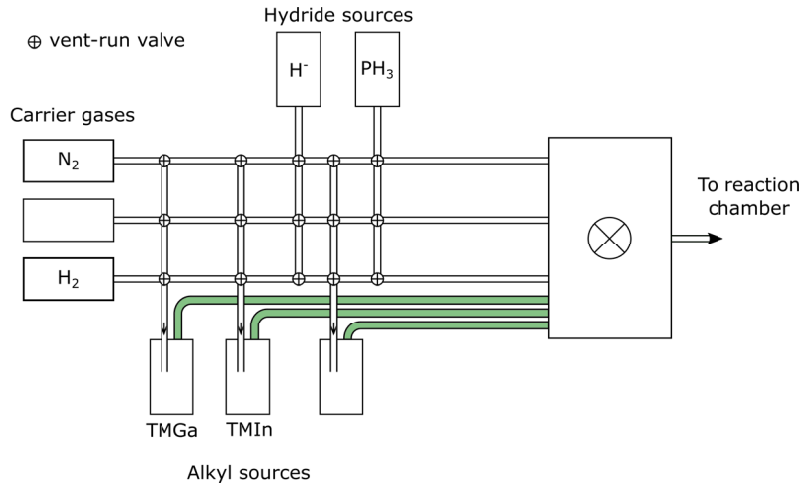

Figure 2: Gas delivery system of a MOCVD reactor.

In Figure 2 the semiconductor sources are stored in stainless steel bubblers. The alkyl sources used for gallium, indium, phosphide, and aluminium alloys are typically e.g. trimethylgallium (TMGa), triethylindium (TMIn), phosphine (PH_3), and trimethylaluminium (TMAl). In the process, the carrier gases are passed through the liquid or over the solid metalorganic alkyl sources [22]. In the bubbler, carrier gas picks up metalorganic vapor and transports it to the reactor. The alloy composition and layer thickness depend on the flow of the gases, thus a constant source delivery is critical to grow lattice-matched, thin film optoelectronic devices. The mass flow of the alkyl is commonly monitored using ultrasonic sensors, and controlled using special vent-run valves. [24]

The gas mixture from the gas delivery system is passed to a high temperature reaction chamber where an appropriate substrate is located. Suitable substrates for III-V semiconductor growth are wafers like silicon, silicon carbide, zinc oxide and sapphire [23]. Figure 3 shows a simplified schematics diagram of MOCVD reaction chamber.
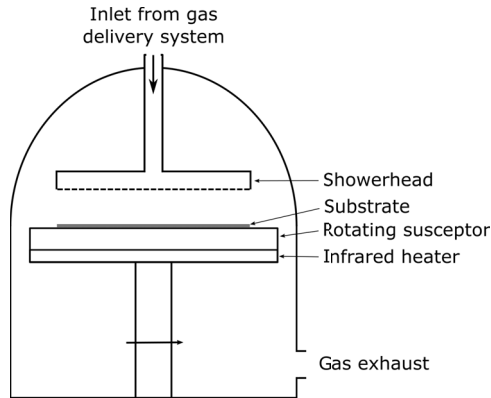
Inlet from gas
delivery system

Showerhead
Substrate
Rotating susceptor
Infrared heater

Gas exhaust

Figure 3: A simplified schematic diagram of a MOCVD reaction chamber.

The gas chamber as shown in Figure 3 is a vessel in which the gas mixture from the gas delivery system shown in Figure 2 is introduced into a heated substrate. To improve the uniformity of the normal gas flow, the gas is delivered to the chamber through a showerhead diffuser. To improve the uniformity of the epitaxial layer growth, the substrate is rotated. [24]

The simplest case of a pyrolysis reaction introduced in MOCVD is the reaction of an organometallic compound and a gaseous hydride [22]. GaAs is a widely used optosemiconductor, emitting and absorbing infrared radiation at wavelengths above 800 nm. It is used in light-emitting diodes as well as in high efficiency multi-junction solar cells. The most common example of such a reaction is the growth of GaAs from metalorganic trimethylgallium $(CH_3)_3Ga$ and arsine AsH_3

$$(CH_3)_3Ga + AsH_3 \rightarrow GaAs + 3CH_4. \tag{1}$$
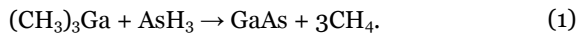
In this work, we have studied the optical emission and absorption spectral properties of a GaAs optosemiconductor device manufactured using MOCVD. Other technologically important III-V optosemiconductors, such as GaN, $Al_xGa_{1-x}As$, and InGaAlP can also be grown using similar MOCVD process with TMGa, TMAl, and TMIn as alkyl sources [22, 24, 25].

2.2 Band gap

The band gap of a semiconductor is an energy difference between the valence and conduction bands where no electron can exist. When an electron annihilates with a hole, an energy equal to the band gap is released. Thus, the band

gap energy characterizes the optical emission or absorption spectrum of the semiconductor device. The band gap energy, and thus the wavelength of the emitted or absorbed light, depends on the materials used and whether the band gap is direct or indirect. Figure 4 shows the schematic diagrams of the band structures of a direct and an indirect band gap.
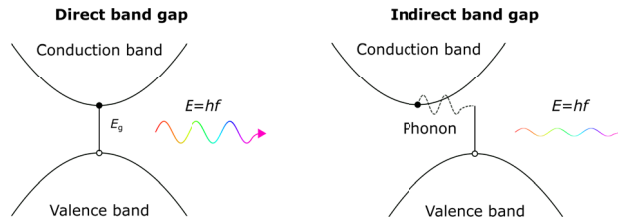

Figure 4: Semiconductor band gap can be either direct or indirect. The vertical and horizontal scales describe electron energy and momentum, respectively.

In radiative recombination, an electron in the conduction band annihilates a hole in the valence band, releasing a photon. As shown in Figure 4, the semiconductor band gap can be either direct or indirect. In direct band gap semiconductors, the momentum of the electron at the conduction band equals the momentum of the hole at the valence band. In the case of direct band gap, all energy is released in the form of a photon. In indirect band gap semiconductors, the energy minimum of the conduction band has different momentum as the energy maximum of the valence band. As the momentum of a photon is $p = E/c$, to satisfy conservation of energy and crystal momentum, emission or absorption of a phonon (quantum of lattice vibration) must also be involved. It is much less likely for a phonon to occur than to not occur, thus the quantum efficiency of semiconductors with an indirect band gap is considerably lower than in direct band gap semiconductors. [26]

The value for the band gap energy of a semiconductor device depends on the materials used. In ternary (three different elements) and quaternary (four different elements) alloys, the band gap also depends on the alloy composition or ratio of the number of different atoms. In addition, the band gap energy has highly temperature dependent characteristics. Thus, to determine the band gap energy of a sample, the temperature of the p-n junction need to be known and stabilized. [27]

The band gap energy of a material can be determined using several techniques such as based on spectral absorption [28, 29], reflectance [30], photoluminescence [31-35], or quantum efficiency [36, 37]. To determine the band gap of a material, the sample needs to be characterized as a function of energy. When determining the material band gap using absorption spectrum measurement,

the absorption coefficient α_a as a function of energy is measured. The band gap energy can be evaluated using a Tauc plot of $(h\nu\alpha_a)^2$ as a function of photon energy $h\nu$. The analysis is carried out by extrapolating the linear region of the rising edge of the Tauc plot and noting the energy value where this line drops to zero [29]. Using spectral reflectance for band gap determination, the absorption of the material is calculated from the reflectance data and the Tauc plot is utilized to find the band gap energy [30]. Both the spectral absorption and spectral reflectance of a material can be measured using a spectrophotometer.

In photoluminescence based band gap determination methods the sample is excited by laser radiation with a photon energy larger than the band gap energy and the photoluminescence signal is measured with a spectroradiometer [34]. The band gap energies can be determined using the peak energy of the photoluminescence intensity [35].

To determine the material band gap energy from quantum efficiency measurements, the spectral electrical quantum efficiency of the sample needs to be measured. The measurement can be carried out by using a grating monochromator as a monochromatic light source and measuring the electrical current signal of the sample as a function of energy. The band gap can be determined from the measurement results by fitting exponential functions of the form $\exp\{a + bE\}$, with fitting parameters a and b, to the data at the band edge and to the saturation region of the quantum efficiency. The band gap is determined as the intersection point of the exponential fits. [37]

The band gap energy of a material at high temperatures (>290 K) cannot be determined as precisely as at low temperatures because the spectral properties are thermally broadened [38]. In this thesis we have developed a method to characterize a temperature-invariant parameter related to the band gap energy. As the band gap energy depends on the alloy composition, we also demonstrated in publication III that the alloy composition can be determined from the band gap energy when the alloy is known.

2.3 High power LEDs

Incandescent light bulbs have been the traditional way to produce light for more than hundred years. From their invention until the beginning of the third millennium, LEDs were mainly used as indicator lights. The first generation of white LEDs were packed to similar packages as indicator LEDs and demonstrated the concept of white LED from a phosphor-coated semiconductor. [39]

The interest of using LEDs for illumination applications started to grow at the first decade of 21st century, after commercializing high-power white LEDs producing over hundred times the optical flux of indicator-style LEDs. The high light output of white LEDs was achieved using large dies, high driving currents, and efficient heat extraction methods from the semiconductor junction to the heat sink. [39]

White LEDs can be manufactured with two different approaches, LED-based or LED-plus-phosphor-based [40]. In the LED-based approach, two, three, or four LEDs with different band gaps (emission peak wavelengths) are combined to produce white light. In the phosphor-based approach, a blue or ultraviolet (UV) LED is coated with phosphor, commonly yellow cerium-doped yttrium-aluminum-garnet (Ce:YAG), absorbing part of the blue/UV photons and emitting them at higher wavelengths. Nowadays, the most widely used approach to manufacture commercial white LEDs is the phosphor-converted method based on an InGaN blue LED chip and $Ce^{3+}:Y_3Al_5O_{12}$ (Ce:YAG) yellow phosphor [41]. Figure 5 shows a cross section of a white LED.
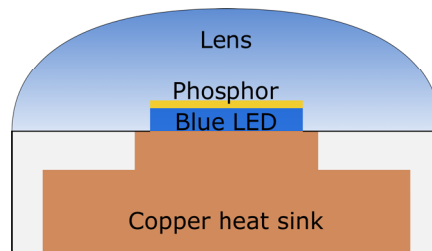
Figure 5: Cross section of a typical white LED.

The electrical power of modern LED chips used in illumination applications is between 1 and 5 W, and the area of the semiconductor chips typically smaller than 1 mm², corresponding to a heat flux of higher than 100 W/cm² [9]. Due to the small area and high power of the chip, efficient thermal management for the LED device is required. As seen in Figure 5, in a typical high power LED, the semiconductor chip is attached to a heatsink. In addition, high power LEDs require a heat conductive circuit board and a heat sink to efficiently remove the heat from the LED chip. The lifetime and output intensity of an LED have been shown to depreciate with increasing temperature [42, 43]. According to the LED datasheets, the absolute maximum rating is typically in the range between 125 °C and 150 °C.

As the lifetime of an LED depends highly on the temperature, the reliability of the packaged LED strongly depends on the die attach quality. Any impurity or defect between the die and the heat sink may cause temperature increase in the

LED, leading eventually to failure in the operation [44]. In domestic LED lamps, passive cooling using an aluminum heat sink and convective heat transfer is the most used cooling method, but the amount of heat dissipated is limited. For scientific and advanced high power LED applications, various studies on other thermal management methods such as based on liquid cooling [45], heat pipes [46], liquid metal [47], or micro-jet arrays [48] have been performed. These methods are more efficient in removing heat from the die, but they are complex and expensive, limiting their use in most consumer applications.

In publications I to III, the effect of temperature on the lifetime and optical characteristics of LEDs was studied.

2.4 Multi-junction solar cells

Multi-junction solar cells are solar cells made of III-V semiconductors comprising of at least two layers of different alloys. In multi-junction solar cells each p-n junction absorbs a separate portion of the solar energy spectrum, allowing for solar energy conversion with efficiencies as high as 46% [49]. III-V solar cells are manufactured using similar epitaxial growth techniques as LEDs. The elements used are relatively rare, such as indium and gallium, which makes III-V solar cells orders of magnitude more costly than silicon solar cells [10, 50]. Due to the high price of III-V solar cells, their use has been limited to applications in space technology where high efficiency and low weight combined with reliability are required [10].

Some terrestrial applications are presently considered in addition to space applications, such as MJSC use with solar concentrator technologies [10] and energy harvesting applications under indoor lighting conditions[11]. By concentrating the solar irradiance to 1000 times the terrestrial solar irradiance of 1000 W/m2, less semiconductor surface is needed and thus more reasonable costs are achieved. Recent studies have also suggested new applications for high efficiency III-V solar cells in energy harvesting systems. Network connected sensors and devices without batteries or wired power supplies would be beneficial in indoor conditions, where ambient light is nowadays produced using light emitting diodes or fluorescent lamps. Due to the flexibility of the band gap energy values of III-V solar cells, MJSCs can produce more electricity per surface area under indoor lighting conditions than traditional silicon solar cells. [11]

In monolithic MJSC, the different layers are epitaxially grown on one substrate and the sub-cells are interconnected in series by tunnel diodes. The sub-

cells of monolithic MJSCs are not accessible separately, which makes character-ization and measurement procedures challenging [51].

In 2014, the most efficient multi-junction solar cells comprising of four junc-tions achieved the efficiency of 44.7% at 247-times concentration of the solar irradiance [52]. The cell sample used in [52] was a four-junction prototype de-vice comprising of two mechanically stacked double-junction devices, but typi-cally the high efficiency III-V multi-junction solar cells comprise of three epi-taxially grown layers [26]. Figure 6 shows the simplified layer structure of a tri-ple-junction solar cell.
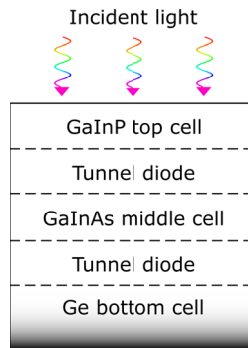
Figure 6: Schematic structure of a GaInP-GaInA-Ge triple-junction solar cell.

In Figure 6, the GaInP, GaInAs, and Ge subsells are stacked on top of each other and interconnected by tunnel diodes. The layers are arranged in such a way that each subcell has a higher band gap than the one below it. As each junc-tion absorbs light from a spectral range closest to its band gap, thermal losses are minimized. [26]

Separating electrically the signals generated by different layers is not straight-forward and the large number of layers in III–V MJSC structures makes pure experimental optimization very expensive and protracted. Optimization is cur-rently performed by predictive numerical modelling, which suffers from the lack of III-V material properties data. The effect of junction temperature on the op-tical characteristics of III-V multi-junction solar cells was studied in publication IV.

3. Optical characterization

This chapter describes the methods utilized to carry out the practical measurements of the scientific articles of this thesis. Before the more detailed descriptions of the used devices and measurement setups, the terms radiometry and photometry should be clarified. Radiometry is a set of techniques to measure electromagnetic radiation, in this thesis optical radiation between ultraviolet and infrared. In photometry, electromagnetic radiation is measured as well, but limited to visible light only, and weighted as perceived by the human eye. In the case of this thesis, the measurements carried out for individual LEDs and III-V solar cells are radiometric measurements, whereas the measurement carried out for LED lamps are photometric measurements.

3.1 Luminous efficacy measurements of LED lamps

Luminous flux is a measure of the total amount of visible light a light source emits. The SI unit for luminous flux is lumen [lm] and the measurement is carried out with defined solid angle which is often 4π. For example in 2017, the luminous flux of a retrofit 8.5 W LED lamp equivalent to a 60 W incandescent lamp is about 800 lm. For LEDs, used in energy efficient lighting, the luminous efficacy [lm/W] is typically the most interesting quantity, describing how many lumens per electrical watt is produced.

Luminous flux and luminous efficacy are typically measured using a setup based on an integrating sphere [53-55]. The integrating sphere is a spherical device with its interior covered with a white diffuse coating, typically with barium sulfate ($BaSO_4$) [56]. Figure 7 shows the luminous efficacy measurement setup developed at Aalto University that was used in this work [57].
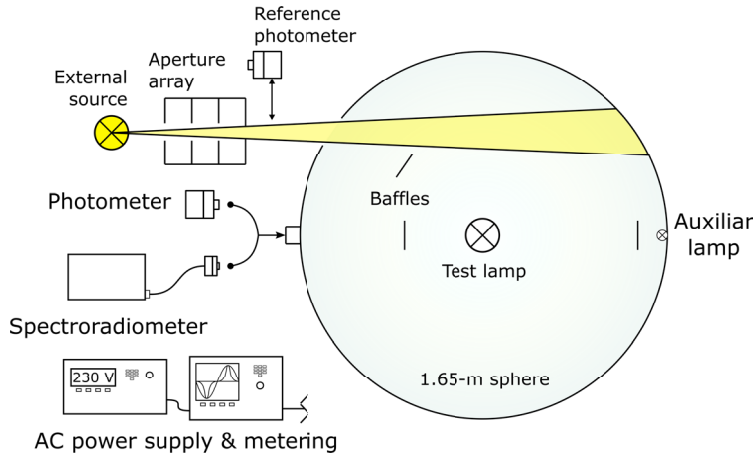
Figure 7: Luminous efficacy measurement setup.

The luminous efficacy setup shown in Figure 7 comprises of a 1.65-m integrating sphere, external light sources for calibration and correction, and the detectors and meters for light and electricity measurements. The direct exposure of the photometer and spectroradiometer heads are blocked using a baffle between the detector and the test lamp. A baffle is also used to prevent the light emitted by the device under test from exiting the sphere through the reference input port.

To study the possible decrease of luminous flux, and the possible changes in spectral quantities during aging of an LED, a measurement setup as in Figure 7 was used in publication II. All the measurement devices in the setup were traceable to the photometric scale of the Metrology Research Institute (MRI) of Aalto University. Figure 8 shows a photograph of the integrating sphere used.

Figure 8: Photograph of the integrating sphere setup used to measure the absolute photometric quantities of LED lamps.

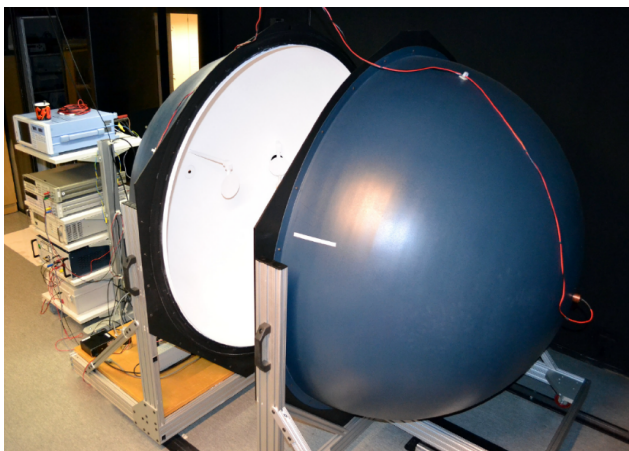Before measurements, the responsivity of the setup needs to be characterized using an external light source and a reference photometer [58]. The illuminance [lm/m²] from the external source passing into the sphere is measured using the reference photometer [59]. As the area of the aperture through which the light passes into the sphere is known, the luminous flux can be calculated using the signal of the reference photometer and the aperture area. The signal of the sphere photometer is compared with the signal of the reference photometer, resulting in the luminous flux responsivity of the integrating sphere setup. In addition, corrections for light distribution and test lamp spectrum are needed [55, 57].

The 230 V 50 Hz operating voltage for the test lamp is supplied using a programmable AC power supply. The electrical power of the test lamp was measured using a calibrated power analyzer. The luminous efficacy [lm/W] was calculated by dividing the measured luminous flux [lm] by the active electrical power [W]. The expanded uncertainty (k=2) of the absolute luminous efficacy measurements carried out in publication II was 1.2% [55].

3.2   Measurement of emission spectrum

In the integrating sphere setup shown in Figure 7, the relative spectral radiant flux of the test lamp is measured using a spectroradiometer by replacing the photometer head with a spectroradiometer head in the detector port. The absolute spectral radiant flux can be calculated using the relative spectral data and the luminous flux value measured with the photometer using relation [60]

$$\Phi_{\mathrm{v}} = K_{\mathrm{m}} \int \Phi_{\mathrm{e}}(\lambda) V(\lambda) d\lambda \,, \qquad (2)$$

where Φ_{v} is the measured luminous flux, K_{m} = 683.002 lm / W is the maximum luminous efficacy of photopic vision, Φ_{e} is the absolute radiant flux spectrum, and λ is the wavelength. The relative radiant spectrum is multiplied with a constant to match the equation, resulting in the absolute spectral radiant flux Φ_{e}. The luminous efficiency function $V(\lambda)$ describes the relative spectral responsivity of a human eye [61]. In addition to the radiant flux, colorimetric properties, such as color coordinates and correlated color temperature (CCT) for the test lamp can be calculated using the spectral data.

In this work, emission spectra of individual LEDs and III-V solar cell samples were measured. The measurement setup in Figure 7 is capable of absolute measurements of luminous flux and spectral radiant flux. However, when measuring

semiconductor devices for optical parameter characterization, absolute measurements are typically not essential. Measurement of relative spectra of components with a calibrated spectroradiometer is often sufficient. It is then important that spectral radiant intensity values at different wavelengths have the correct ratio. This can be achieved with absolute calibration of the spectroradiometer.

In the publications I, III, and IV, the spectral properties of the optosemiconductor devices were measured at relative scale. An example measurement setup for such a measurement is presented in Figure 9.
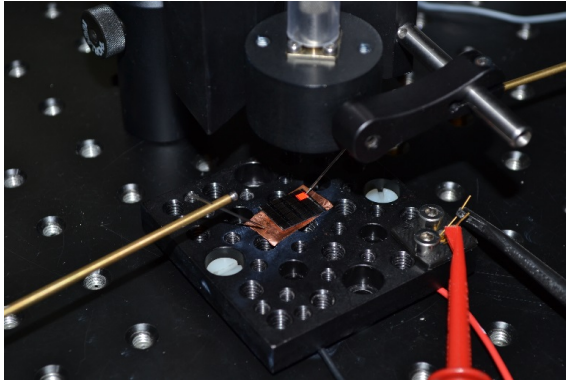

Figure 9: Relative spectral irradiance measurement of a III-V solar cell. The solar cell sample is attached on a temperature controller mounting plate, below the diffuser head of the spectroradiometer.

Figure 9 shows the relative spectral irradiance measurement setup for III-V solar cells to determine the temperature dependence of the optical characteristics of the samples. The measurement setup comprised a spectroradiometer based on a CCD (Charged-Coupled Device) detector and a temperature controlled mounting base. A diffuser head and an optical fiber were used to carry the light signal emitted by the cell to the spectroradiometer. The temperature of the mounting base was controlled using a Peltier element and a thermoelectric cooling controller. Micropositioners with tip diameters of 5 μm were used for the electrical contacts to the semiconductor wafer.

In publication I, a measurement facility was developed to measure the temperature dependence of the optical characteristics of high power LEDs. The power of LEDs used for illumination can be several watts, from which even 80% will be wasted in the form of heat [62]. To study the effect of temperature on the transient and steady state characteristics of high power LEDs, cooling power of tens of times higher than the heating power of the LEDs is required [63]. Such high cooling powers are not available using a Peltier element and controller of a

reasonable size. To overcome the limitations of the Peltier elements, a temperature controller for high power LEDs based on liquid cooling and resistive heating was built in publication I. The developed measurement facility was later used to carry out the spectral measurements used in publication III and in [64].

3.3   Spectral responsivity measurements

The spectral responsivity of a solar cell in the units of A/(Wnm^{-1}) indicates the amount of current the cell produces when irradiated with a light at a particular wavelength. The spectral responsivity of a solar cell can be used to evaluate the current produced by the cell when exposed to sunlight with known spectral distribution [65].

To study the effect of temperature on the optical characteristics of III-V optosemiconductors, multi-junction III-V solar cells were measured for their emission and absorption spectrum in publication IV. The absorption spectrum was measured using a reference spectrometer based on a grating monochromator as in [66]. The measurement setup comprised a halogen light source, computer-controlled monochromator, and a motorized linear translator for sample and reference detector movement. The reference detector used was a calibrated silicon trap detector manufactured by Aalto University [67]. Figure 10 shows a simplified schematics diagram of the reference spectrometer setup.
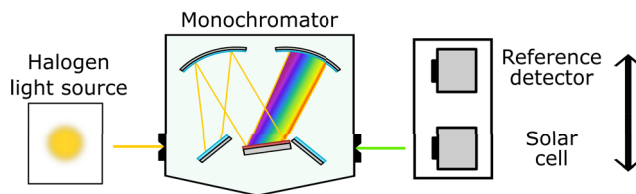
Figure 10: Schematics of the reference spectrometer used for spectral responsivity measurements of the solar cells.

In Figure 10, the white light from the halogen source is passed through the monochromator to form a monochromatic beam for the solar cell sample. The reference detector and the solar cell were alternately placed in the measurement beam using a linear translator. The current signal from the reference detector and the solar cell sample were measured using a high-precision current-to-voltage converter. After the subtraction of the dark signals from the readings, the spectral responsivity of the solar cell sample was determined as

$$R_{s\lambda} = \frac{Y_{s\lambda}}{Y_{r\lambda}} R_{r\lambda} ,$$ (3)

19

where $Y_{s\lambda}$ is the output current of the solar cell sample, $Y_{r\lambda}$ is the output current of the reference detector, and $R_{r\lambda}$ is the known spectral responsivity of the calibrated reference trap detector.

3.4   Lifetime projection of high power LEDs

The luminous flux and spectral properties of an LED changes with time [68]. In publication II, the lifetimes of LEDs were studied using natural and accelerated aging tests. Commercial LED lamps, comprising high power LEDs in conjunction with power electronics were used in the study. The natural aging at room temperature was carried out by the author using the luminous efficacy measurement setup described in chapter 3.1. The accelerated aging tests at elevated temperatures of 45 °C and 60 °C were carried by Laboratoire National de Métrologie et d'Essas (LNE) in France.

In the aging test, five different types of LED lamps were aged at room temperature and at the elevated temperatures of 45 °C and 60 °C. The lamps aged at room temperature were measured at regular intervals for 50 000 h. The lamps were measured for luminous flux, spectral radiant flux, and electrical power using the setup as in [55]. Figure 11 shows the decay of the luminous flux of the studied lamps aged at room temperature.
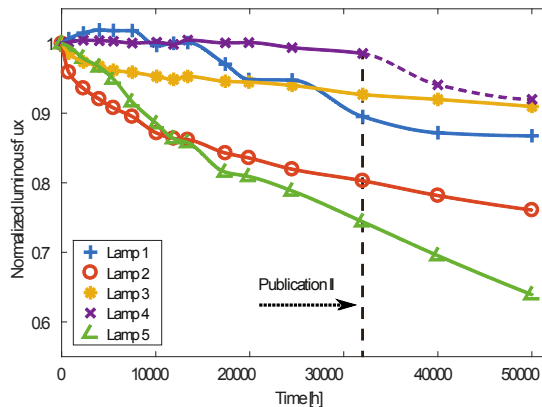
Figure 11: Decay of the luminous flux of five different types of commercial LED lamps during 50 000 h (~6 years) of continuous burning. Four samples of each type were measured, and the average luminous flux was calculated. The markers indicates the measurement points.

The decay of luminous flux as shown in Figure 11 was earlier published in publication II. However, since the earlier publication, 20 000 h more measurement data is included. The lifetime of the LED light sources used in general lighting is defined as L_{70} lifetime, which is based on the time for 70% light output degradation [69]. As shown in Figure 11, this limit has been reached by the lamp type

5 after 35 000 h of continuous burning. In publication II, the average lifetime for the lamp type 5 was predicted to be 33 300 h, which agrees well with the measurement value of 35 000 h. Two from four samples of the lamp type 4 failed after 40 000 h. The electrical power consumption was measured and logged as well and it stayed rather constant. Thus, the degradation of luminous flux is mainly due to the aging of the LEDs as shown in publication II.

As seen in Figure 11, excluding lamp type 5, the lifetimes of the other samples can be estimated to be more than 100 000 hours. Worth mentioning is the sample type 4, the luminous flux of which stayed almost constant for the first 30 000 hour of continuous burning, after which two samples failed and the average luminous flux started to depreciate.

Thermal aging using elevated ambient temperatures is a widely used method to accelerate the aging of electronic devices [39, 70, 71]. In a hammer test, the device under test is subjected to extreme temperature variations to break the device in a reasonable period of time [72, 73]. The intensity of indicator-style LEDs can degrade very rapidly, reaching a 50% light output level within 10 000 h [74]. However, the lifetimes of high power LEDs can be even higher that 100 000 hours, it is not possible, or at least not practical to carry out measurements over such long periods. According to publication II, to get a reliable data from natural aging data, aging time of more than a year is required.

To overcome the requirement for a long aging period in natural aging, increased aging temperatures can be used to accelerate the aging. As the lifetime of light-emitting diodes has been shown to decrease with increasing temperature [75-79], an accelerating factor can be calculated to project the lifetime of an LED light source aged at different temperature than the temperature at operating conditions. The depreciation of luminous flux of high power LEDs has been shown to follow the exponential curve of the form

$$\Phi(t) = B \exp(-\alpha t), \tag{4}$$

where $\Phi(t)$ is the luminous flux at time t, B is a fitting constant, α is the decay rate of the luminous flux.

When aging LEDs at different temperatures, different decay constants α are achieved. The Arrhenius equation is a widely used formula for temperature dependence of exponential phenomena and suggested to be utilized to approximate the effect of temperature on the aging of high power LEDs [78, 80, 81]. The Arrhenius equation gives a decay rate α_i at a temperature T_i, when the pre-exponential factor A and activation energy E_a are known

$$\alpha_i = A \exp\left(-\frac{E_a}{k_B T_i}\right), \qquad\qquad (5)$$

where k_B is the Boltzmann constant. The pre-exponential factor A and the activation energy E_a are constants which can be solved using two aging measurements carried out at different temperatures.

In addition to accelerating the aging with elevated temperatures, acceleration has been implemented using higher current stress levels [82, 83]. In these studies the decay of the output luminous fluxe was used as the aging criterion as well.

As the lifetime of an LED light source highly depends on the junction temperature, the most dominant factor influencing the lifetime of the LED is the thermal management of the device [84,85]. High temperature will cause the decrease of lifetime due to several reasons such as degradation of the phosphorus layer [86], browning of the epoxy resin covering the chip [87, 74], cracking of the die [88], or breaking of the bonding wires and contacts [86]. In addition to the failure of the LED chip, breaking of the driving electronics due to the high temperature or wear-out failure of aluminium electrolytic capacitors or solder joint fatigue is a remarkable cause for a failure of an LED lamp [89]. Thus, the lifetime of an LED light source is mainly depending on the thermal management of the device. The manufacturer lifetimes for costly LED lamps with a massive aluminium heat sink can be tens of thousands of hours, whereas the lifetime expectancy for an LED lamp without a metal heat sink is typically around 15 000 hours.

To study the lifetime of LED light sources, LED lamps were aged at room temperature and at two elevated temperatures of 45 °C and 60 °C in publication II. Calculating the acceleration of aging as the drop of luminous flux, the aging was on the average 1.35 times faster at the elevated temperature of 45 °C and 2.36 times faster at the temperature of 60 °C, compared to the speed of aging at room temperature. Despite the elevated temperature, none of the studied samples failed during the accelerated aging period of 6 months.

3.5 Characterization of LEDs using the emission spectrum

The emission spectrum of an LED is generated by electron-hole recombination, and the central wavelength of the spectrum depends on the band gap energy as shown in Chapter 2.2. The spectral shape $I(E, T)$ can be modelled as a product

of the joint density of states of electrons and holes and the Maxwell-Boltzmann distribution [1, 64]

$$I(E,T) \propto f\left(E - E_{\mathrm{g}}(T)\right) \times e^{-\frac{E - E_{\mathrm{g}}(T)}{k_{\mathrm{B}}T}}, \tag{6}$$

where f is the joint density of states, E is the photon energy, and $E_{\mathrm{g}}(T)$ is the band gap energy at junction temperature T. For a typical III-V optosemiconductor device, the temperature dependent band gap energy $E_{\mathrm{g}}(T)$ has been measured to follow a second order Varshni equation [34, 90]. For temperatures $T \gg 0$ K, the temperature dependence of the band gap can be approximated by a linear equation [91]

$$E_{\mathrm{g}}(T) = E_{\mathrm{B}} - p k_{\mathrm{B}} T, \tag{7}$$

where E_{B} represents the linearly extrapolated band gap energy at 0 K, and p is a positive constant defining the band gap shift of the LED as a function of temperature.

As shown in publication III, when normalizing the modeled spectra, Eq. (6), at different temperatures, it can be concluded that at the photon energy E_{B}, the relative intensity does not depend on temperature, i.e. the spectra intersect at a fixed energy value E_{B}. The emission spectrum model (6) is only a rough model of the shape of the emission spectrum, and it is valid to the high-energy (low wavelength) side of the spectrum only. However, this intersection energy can be found in the measured emission spectra as well. Figure 12 shows the measured and modelled spectra of a white LED at different temperatures.
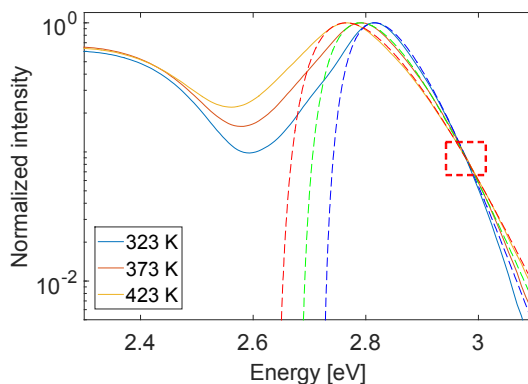

Figure 12: Normalized measured (solid lines) and modelled (dashed lines) spectra of the blue peak of a white LED at different temperatures between 323 K and 423 K. The temperature invariant energy value E_{B} is inside the red rectangle.

In publication III, the temperature-invariant intersection energy E_B was shown to be the linearized extrapolation of the band gap energy from room temperature to 0 K. For a typical GaN LED, the difference between the band gap energy at 0 K temperature and the intersection energy E_B was found to be less than 2%. The measurement uncertainty of the energy value E_B was shown to be less than 0.2%. In addition to the fixed energy value, the relative intensity of the intersection point was fixed as well. Thus, it was considered in publication III that the intersection energy E_B can be utilized as a wavelength and intensity reference.

As the band gap of a material depends on the alloy composition of the semiconductor material, it was suggested in publication III, that the alloy composition of the semiconductor material may be determined using the fixed intersection energy E_B. More specifically, when two elements occupying a certain lattice position are known, the method can determine the ratio of the occupancy by these elements. One of the measured LED samples in publication III was an InGaN blue LED, manufactured by Aalto University using MOCVD. The targeted In content of the LED was 15%, but the authors in [92] measured the In content to be 18% using X-ray diffraction. In publication III, the alloy composition of the InGaN LED was determined to be 18% as well using the E_B energy.

3.6 Measuring band gap energies of III-V LEDs and solar cells

In publication IV, the temperature dependence of the optical band gap of a GaAs / GaInP double-junction solar cell manufactured using MOCVD as in [52] was studied. In addition to the epitaxially grown double-junction sample, separate single-junction GaAs and GaInP samples were measured for temperature dependence of the optical band gap. As III-V solar cells are manufactured using the same materials and processes as III-V LEDs, solar cells can be used as light-emitting devices as well. All samples were thus measured for both emission and absorption spectra, and the results were compared. The emission and absorption spectra of the double-junction cell are shown in Figure 13.
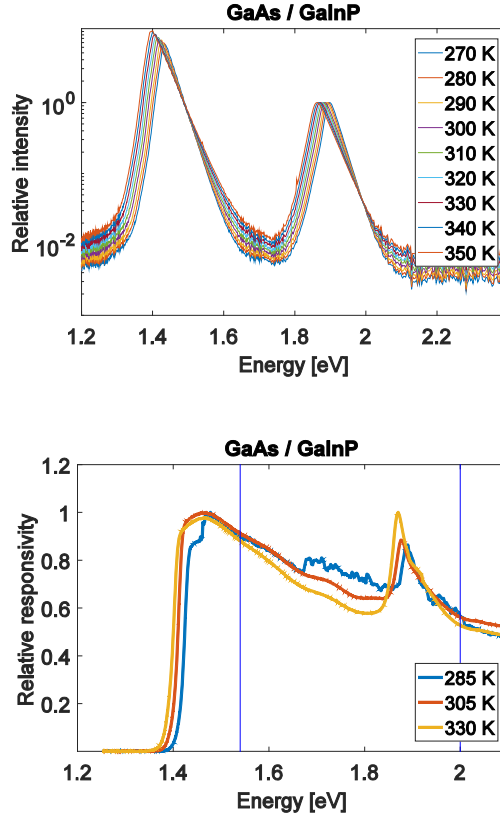
Figure 13: Emission (upper) and absorption (lower) spectra of a double junction GaAs / GaInP solar cell measured at different temperatures. The emission spectra are normalized to the peak of the GaAs junction. The absorption spectra were normalized to the maximum response of the GaInP junction.

The vertical lines in the spectral responsivity graph in Figure 13 are located at the intersection energies E_B determined from the emission spectrum measurements. The band gap of the spectral responsivity, determined as the rising edge of the measurement data, shifts towards the E_B energy with decreasing temperature.

The band gap energy and its temperature dependence for GaAs is well characterized in literature. The linear extrapolation of the second order Varshni temperature dependence of GaAs band gap from 305 K to 0 K yields a value of 1.56 eV [34, 93]. The E_B energy for GaAs determined from the emission spectrum measurements shown in Figure 13 is 1.54 eV which deviates less than 1.5% from the linearized band gap energy at 0 K.

For the two-element III-V compound GaAs, the alloy composition is always $Ga_{0.5}As_{0.5}$, thus the material parameters are well characterized. For GaInP compounds, the band gap energy depends on the alloy composition. In addition to the alloy composition, the band gap of GaInP has been reported to be a function of the lattice order and orientation [94]. In publication IV, values of ~1.96 eV

[95] and 1.985 eV [96] for the band gap energy at 0 K temperature were found for similar samples to ours. The latter reference provides information to calculate the linear approximation of the band gap energy around 305 K and to extrapolate it to 0 K, yielding E_B = 1.994 eV. From the emission spectrum measurement results shown in Figure 13, we can determine the E_B energy for GaInP to be 1.990 eV.

In publication IV, three different samples were measured, a double-junction GaAs / GaInP, and single-junction GaAs and GaInP samples. The intersection energies were determined for all samples, and they are summarized in Table 1. As can be seen, the measured values are close to the literature values. The E_B values measured for the single-junction samples are also congruent with the values measured for the double-junction sample.

Table 1: Band gap energies of the III-V solar cell samples used in publication IV.

Band gap energy [eV]	GaAs (single junction)	GaAs (double junction)	GaInP (single junction)	GaInP (double junction)
E_B from emission spectrum measurements	1.54	1.54	2.00	1.99
E_B from literature [34, 96]	1.56	1.56	1.99	1.99

4. Conclusions

In this thesis, measurement facilities and methods to characterize light-emitting diodes and solar cells manufactured using materials from element groups III and V were developed. Despite the high energy efficiency of LEDs, most of the electrical input power will be wasted in the form of heat. To measure the temperature dependence of the optical characteristics of high power LEDs, a temperature controller based on liquid cooling and resistive heating was built. Such system provided cooling power of tens of watts, enough to cool down high power LEDs within seconds. The measurement setup was later used in several emission spectrum measurements carried out in this thesis at varied temperatures.

The lifetime of LED lamps based on high power LEDs can be tens of thousands of hours, as specified by manufacturers. Due to the long expected lifetimes of even ten years of continuous burning, the real practical lifetime of LED lamps and high power LEDs has been difficult to measure. In this thesis, 20 samples of LED lamps were aged for ~6 years. During the aging, only two samples failed. In the case of a failure of an LED lamp, the failed component was not the LED chip, but the electronics driving the LEDs inside the lamp. The same types of LED lamps were aged at elevated temperatures of 45 °C and 60 °C as well. According to the aging results carried out at the elevated temperatures, the aging of the LEDs is 1.35 times faster at the temperature of 45 °C and 2.36 times faster at the temperature of 60 °C, for the samples studied. The aging at the elevated temperatures lasted 6 months, during which none of the samples failed. The aging measurements carried out in this thesis also showed that the lifetime of high power LEDs, defined as the time when the luminous flux has decreased to 70% of the initial value, can be even longer than the manufacturer specifications.

The band gap energy and thus the peak wavelength is one of the most important parameters of LEDs. For a batch of LEDs to emit light at the same wavelengths, their band gaps need to be uniform. However, the band gap is a heavily temperature dependent characteristics and varies between LED samples of the

same type. Traditional methods to measure the band gap energy of an optosemiconductor require the junction temperature of the sample to be known and stabilized. In this thesis, a method to characterize a temperature-invariant parameter describing the band gap energy of III-V optosemiconductors was introduced and demonstrated. The relation between the semiconductor alloy composition and the band gap parameter has been widely studied earlier. Utilizing the temperature-invariant band gap energy demonstrated in this thesis, the alloy composition of a ternary alloy LED was determined.

Modern high efficiency solar cells are based on the same manufacturing technology and materials as high power LEDs. The efficiency of III-V solar cells is based on stacking multiple semiconductor layers with different material compounds and band gap energies on top of each other. Separating the junction, and measuring the band gap characteristics for such multi-junction solar cells, has appeared to be challenging. The novel method to determine the temperature-invariant band gap energy of high power LEDs was demonstrated to work for III-V multi-junction solar cells as well. By utilizing the method, the different layers of the sample can be easily separated.

References

[1] B.-L. Ahn, C.-Y. Jang, S.-B. Leigh, S. Too, and H. Jeong, "Effect of LED lighting on the cooling and heating loads in office buildings," Appl. Energy 113, 1484-1498 (2014).

[2] E. Tetri, A. Sarvaranta, and S. Syri, "Potential of new lighting technologies in reducing household lighting energy use and CO_2 emission in Finland," Energ. Effic. 7, 559-570 (2014).

[3] E. Tetri, S. B. Chenani, R.-S. Räsänen, H. Baumgartner, M. Vaaja, S. Sierla, L. Tähkämö, J.-P. Virtanen, M. Kurkela, E. Ikonen, L. Halonen, H. Hyyppä, and I. Kosonen, "Tutorial: Road Lighting for Efficient and Safe Traffic Environments," LEUKOS, doi: 10.1080/15502724.2017.1283233 (2017).

[4] G. Perino and T. Pioch, "Banning incandescent light bulbs in the shadow of the EU Emission Trading Scheme," Clim. Policy, Advance online publication, doi: 10.1080/14693062.2016.1164657 (2016).

[5] Statista, "Estimated LED penetration of the global lighting market from 2010 to 2020," retrieved 3.3.2017, from https://www.statista.com/statistics/246030/estimated-led-penetration-of-the-global-lighting-market/.

[6] N. Shibata, T. Uemura, H. Yamaguchi, and T. Yasukawa, "Fabrication of LED based on III-V nitride and its applications," Phys. Stat. Sol. 200, 58-61 (2003).

[7] E. F. Schubert, *Light-Emitting Diodes*, University Press, Cambridge, 2010.

[8] M. Vázquez, C. Algora, I. Rey-Stolle, and J. R. González, "III-V Concentrator Solar Cell Reliability Prediction Based on Qauntitative LED Reliability Data," Prog. Photovol. Res. Appl. 15, 477-491 (2007).

[9] J. Wang, X.-J. Zhao, Y.-X. Cai, C. Zhang, and W.-W. Bao, "Experimental study on the thermal management of high-power LED headlight cooling device integrated with thermoelectric cooler package," Energ. Convers. Manage. 101, 532-540 (2015).

[10] S. J. C. Irvine, "III-V Solar Cells," in *Materials Challenges: Inorganic Photovoltaic Solar Energy*, Cambridge: The Royal Society of Chemistry, 2013.

[11] I. Mathews, P. J. King, F. Stafford, and R. Frizzell, "Performance of III-V Solar Cells as Indoor Light Energy Harvesters," IEEE J. Photovoltaics 6, 230-235 (2016).

[12] J. Fan, K.-C. Yung, and M. Pecht, "Lifetime Estimation of High-Power White LED Using Degradation-Data-Driven Method," IEEE Trans. Device Mater. Reliab. 12, 470-477 (2012).

[13] Y. Xi and E. F. Schubert, "Junction-temperature measurement in GaN ultraviolet light-emitting diodes using diode forward voltage method," Appl. Phys. Lett. 85, 2163-2165 (2004).

[14] Y. Xi, J.-Q. Xi, T. Gessmann, J. M. Shah, J. K. Kim, and E. F. Schubert, "Junction and carrier temperature measurements in deep-ultraviolet light-emitting diodes using three different methods," Appl. Phys. Lett. 86, 031907 (2005).

[15] K. Chen, N. Narendran, "Estimating the average junction temperature of AlGaInP LED arrays by spectral analysis," Microelectron. Reliab. 53, 701-705 (2013).

[16] W. L. Ng, M. A. Lourenço, R. M. Gwilliam, S. Ledain, G. Shao, and K. P. Homewood, "An efficient room-temperature silicon-based light-emitting diode," Nature 410, 192-194 (2001).

[17] B. Sørensen, *Solar Energy Storage*, Elsevier Ltd., Oxford, 2015.

[18] K. Chen, R. Kapadia, A. Harker, S. Desai, J. S. Kang, S. Chuang, M. Tosun, C. M. Sutter-Fella, M. Tsang, Y. Zeng, D. Kiriya, J. Hazra, S. R. Madhvapathy, M. Hettick, Y.-Z. Chen, J. Mastandrea, M. Amani, S. Cabrini, Y.-L. Chueh, J. W. Ager III, D. C. Chrzan, and A. Javey, "Direct growth of single-crystalline III-V semiconductors on amorphous substrates," Nat. Commun. 7, 1-6 (2016).

[19] S. Franssila, *Introduction to Microfabrication*, John Wiley & Sons Ltd, Chichester, 2010.

[20] J. W. Matthews, *Epitaxial Growth, Part A,* IBM Thomas J. Watson Research Center, New York, 1975.

[21] P. Battachraya, *Semiconductor Optoelectronic Devices*, Prentice-Hall Inc., Upper Saddle River, 1997.

[22] R. D. Dupuis, "Metalorganic Chemical Vapor Deposition of III-V Semiconductors," Science 226, 623-629 (1984).

[23] T. Lang, *Fabrication of Heteroepitaxial Templates for GaN-based Optoelectronic Devices*, Ph.D. dissertation, Department of Electrical and Communications Engineering, Helsinki University of Technology, Espoo, Finland, 2007.

[24] J. J. Coleman, "Metalorganic Chemical Vapor Deposition for Optoelectronic Devices," Proc. IEEE 85, 1715-1729 (1997).

[25] C. Nozaki, Y. Ohba, H. Sugawara, S. Yasuami, and T. Nakanishi, "Growth temperature dependent atomic arrangements and their role on band-gap of InGaAlP alloys grown by MOCVD," J. Cryst. Growth 93, 406-411 (1988).

[26] A. McEvoy, T. Markvart, and L. Castañer, *Practical Handbook of Photovoltaics: Fundamentals and Applications*, Academic Press, Waltham MA, 2012.

[27] I. Vurgaftman, J. R. Meyer, and L. R. Ram-Mohan, "Band parameters for III-V compound semiconductors and their alloys," J. Appl. Phys 89, 5815-5875 (2001).

[28] N. Ghobadi, "Band gap determination using absorption spectrum fitting procedure," Int. Nano Lett. 3:2, (2013).

[29] N. Soltani, E. Saion, M. Z. Hussein, M. Erfani, A. Abedini, G. Bahmanrokh, M. Navasery, and P. Vaziri, "Visible Light-Induced Degradation of Methylene Blue in the Presence of Photocatalytic ZnS and CdS Nanoparticles," Int. J. Mol Sci. 13, 12242-12258 (2012).

[30] V. Kumar, S. Kr. Sharma, T. P. Sharma, and V. Singh, "Band gap determination in thick films from reflectance measurements," Opt. Mater. 12, 115-119 (1999).

[31] S. Mukai, "Photoluminescent and electrical properties of InGaPAs mixed crystals liquid phase-epitaxially grown on (100) GaAs," J. Appl. Phys. 54, 2635-2645 (1983).

[32] M. Zachau and W. T. Masselink, "Luminescence and Raman measurement of $In_yGa_{1-y}P$ (0.3<y<0.5) grown by gas-source molecular beam epitaxy," Appl. Phys. Lett 60, 2098 (1992).

[33] Y. Ishitani, S. Minagawa, and T. Tanaka, "Temperature dependence of the band-gap energy of disordered GaInP," J. Appl. Phys. 75, 5326-5331 (1994).

[34] E. Grill, M. Guzzini, and R. Zamboni, "High-precision determination of the temperature dependence of the fundamental energy gap in gallium arsenide," Phys. Rev. B 45, 1638-1644 (1992).

[35] S. Mukai, "Photoluminescence and electrical properties of InGaPAs mixed crystals liquid phase epitaxially grown on (100) GaAs," J. Appl. Phys. 54, 2635-2645 (1983).

[36] W. Hadouchi, J. Rousset, D. Tondelier, B. Geffroy, and Y. Bonnassieux, "Zinc oxide as a hole blocking layer for perovskite solar cells deposited in atmospheric conditions," RCS Adv. 6, 67715-67723 (2016).

[37] H. Helmers, C. Karcher, and A. W. Bett, "Bandgap determination based on electrical quantum efficiency," Appl. Phys. Lett. 103, 032108 (2013).

[38] M. Zachau and W. T. Masselink, " Luminescence and Raman measurements of $In_yGa_{1-y}P$ (0.3<y<0.5) grown by gas-source molecular beam epitaxy,"Appl. Phys. Lett. 60, 2098-2100 (1992).

[39] N. Narendran and Y. Gu, "Life of LED-based White Light Sources," J. Disp. Technol. 1, 167-171 (2005).

[40] E. F. Schubert, and J. K. Kim, "Solid-State Light Sources Getting Smart," Science 308, 1274-1278 (2005).

[41] R. Zhang, H. Lin, Y. Yu, D. Chen, J. Xu, and Y. Wang, "A new-generation color converter for high-power white LED: transparent Ce^{3+}:YAG phosphor-in-glass," Laser Photonics. Rev. 8, 158-164 (2014).

[42] F.-K. Wang and T.-P. Chu, "Lifetime predictions of LED-based light bars by accelerated degradation test," Microelectron. Reliab. 52, 1332-1335 (2012).

[43] N. C. Chen, W. C. Lien, Y. K. Yang, C. Shen, Y. S. Wang, and J. F. Chen, "Spectral shape and broadening of emission from AlGaInP light-emitting diodes," J. Appl. Phys. 106, 074514 (2009).

[44] H.-H. Kim, S.-H. Choi, S.-H. Shin, Y.-K. Lee, S.-M. Choi, and S. Yi, "Thermal transient characteristics of die attach in high power LED PKG," Microelectron. Reliab. 48, 445-454 (2008).

[45] Y. Lai, N. Cordero, F. Barthel, F. Tebbe, J. Kuhn, R. Apfelbeck, D. Würtenberger, "Liquid cooling of bright LEDs for automotive applications," Appl. Therm. Eng. 29, 1239-1244 (2009).

[46] X.-y. Lu, T.-C. Hua, M.-j. Liu, and Y.-x Cheng, "Thermal analysis of loop heat pipe used for high-power LED," Thermochim. Acta 493, 25-29 (2009).

[47] Y. Deng, and J. Liu, "A liquid metal cooling system for the thermal management of high power LEDs," Int. J. Heat Mass Transf. 37, 288-791 (2010).

[48] X. Luo, W. Chen, R. Sun, and S. Liu, "Experimental and Numerical Investigation of a Microjet-Based Cooling System for High Power LEDs," Heat Transfer Eng. 29, 774-781 (2009).

[49] M. A. Green, K. Emery, Y. Hishikawa, W. Warta, and E. D. Dunlop, "Solar cell efficiency tables (Version 45)," Prog. Photovoltaics 23, 1-9 (2015).

[50] M. Woodhouse and A. Goodrich, "A Manufacturing Cost Analysis Relevant to Single- and Dual-Junction Photovoltaic Cells Fabricated with III-Vs and III-Vs Grown on Czochralski Silicon," National Renewable Energy Laboratory 2013. http://www.nrel.gov/docs/fy14osti/60126.pdf [accessed on 18 May 2017].

[51] M. Meusel, R. Adelehelm, F. Dimroth, A. W. Bett, and W. Warta, "Spectral Mismatch Correction and Spectrometric Characterization of Monolithic III-V Multi-Junction Solar Cells," Prog. Photovoltaics 10, 243-255 (2002).

[52] F. Dimroth, M. Grave, P. Beutel, U. Fiedeler, C. Karcher, T. N. D. Tibbits, E. Oliva, G. Siefer, M. Schachtner, A. Wekkeli, A. W. Bett, R. Krause, M. Piccin, N. Blanc, C. Drazek, E. Guiot, B. Ghyselen, T. Salvetat, A. Tauzin, T. Signamarcheix, A. Dobrich, T. Hannappel, and K. Schwarzburg, "Wafer bonded four-junction GaInP/GaAs//GaInAsP/GaInAs concentrator solar cells with 44.7% efficiency," Prog. Photovoltaics 22, 277-282 (2014).

[53] Y. Ohno, "Realization of NIST 1995 Luminous Flux Scale Using the Integrating Sphere Method," J. Illum. Eng. Soc. 25, 13-22 (1996).

[54] J. Hovila, P. Toivanen, and E. Ikonen,"Realization of the unit of luminous flux at the HUT using the absolute integrating-sphere method," Metrologia 41, 407-413 (2004).

[55] T. Poikonen, T. Pulli, A. Vaskuri, A. Vaskuri, H. Baumgartner, P. Kärhä, and E. Ikonen, "Luminous efficacy measurement of solid-state lamps," Metrologia 49, S135-S140 (2012).

[56] *The Measurement of Luminous Flux*, CIE 84-1989, International Commission on Illumination, 1989.

[57] T. Poikonen, *Characterization of Light Emitting Diodes and Photometer Quality Factors*, Ph.D. dissertation, Department of Signal Processing and Acoustics, Aalto University, Espoo, Finland, 2012.

[58] Y. Ohno, "Detector-based luminous-flux calibration using the Absolute Integrating-Sphere Method, Metrologia 35, 473-478 (1998).

[59] P. Toivanen, P. Kärhä, F. Manoochehri, and E. Ikonen, "Realization of the unit of luminous intensity at the HUT," Metrologia 37, 131-140 (2000).

[60] T. Pulli, T. Dönsberg, T. Poikonen, F. Manoocheri, P. Kärhä, and E. Ikonen, "Advantages of white LED lamps and new detector technology in photometry," Light Sci. Appl. 4, e332 (2015).

[61] CIE, *Commission Internationale de l'Eclairage Proceedings 1924,* Cambridge University Press, Cambridge, MA, 1926.

[62] B.-L. Ahn, C.-Y. Jang, S.-B. Leigh, S. Yoo, and H. Jeong, "Effect of LED lighting on the cooling and heating loads in office buildings," Appl. Energy 113, 1484-1489 (2014).

[63] Y. Deng and J. Liu, "A liquid metal cooling system for the thermal management of high power LEDs," Int. J. Heat Mass Transf. 37, 788-791 (2010).

[64] A. Vaskuri, H. Baumgartner, P. Kärhä, G. Andor, and E. Ikonen, "Modeling the spectral shape of InGaP-based red light-emitting diodes," J. Appl. Phys. 118, 203103 (2015).

[65] J. Metzdorf, "Calibration of solar cells. 1: The differential spectral responsivity method," Appl. Opt.26, 1701-1708 (1987).

[66] F. Manoochehri, P. Kärhä, L. Palva, P. Toivanen, A. Haapalinna, E. Ikonen, "Characterization of optical detectors using high-accuracy instruments," Anal. Chim. Acta 380, 327-337 (1999).

[67] T. Kübarsepp, P. Kärhä, and E. Ikonen, "Chracterization of a polarization-independent transmission trap detector," Appl. Opt. 36, 2807-2812 (1997).

[68] M. Wager, A. Herzog, H. Ganev, and T. Q. Khanh, " LED aging acceleration – an analysis from measuring and aging data of 14,000 hours LED degradation," Solid State Lighting (SSLCHINA), 2015 12th China International Forum on, 75-78 (2015).

[69] *Approved Method for Lumen Maintenance Testing of LED Light Source*, Illuminating Engineering Society, IES-LM-80-08, USA, 2008.

[70] C.-C. Tsai, J. Wang, M.-H. Chen, Y.-C. Hsu, Y.-J. Lin, C.-W. Lee, S.-B. Huang, H.-L. Hu, and W.-H. Cheng, "Investigaion of Ce:YAG Doping Effect on Thermal Aging for High-Power Phosphor-Converted White-Light-Emitting Diodes," IEEE Trans. Device Mater. Rel. 9, 367-371 (2009).

[71] L. Trevisanello, M. Meneghini, G. Mura, M. Vanzi, M. Pavesi, G. Meneghesso, and E. Zanoni, "Accelerated Life Test of High Brightness Light Emitting Diodes," IEEE Trans. Device Mater. Rel. 8, 304-311 (2008).

[72] J. Zhang, Z. Hai, S. Thirugnanasambandam, J. L. Evans, M. J. Bozack, Y. Zhang, and J. C. Suhling, "Thermal Aging Effects on the Thermal Cycling Reliability of Lead-Free Fine Pitch Packages," IEEE Trans. Compon., Packag. Manuf. Technol. 3, 1348-1357 (2013).

[73] Research Triangle Institute, *Hammer Testing Findings for Solid-State Lighting Luminaires*, Research Triangle Park, NC, 2013.

[74] N. Narendran, Y. Gu, J. P. Freyssinier, H. Yu, and L. Deng, "Solid-state lighting: failure analysis of white LEDs," J. Cryst. Growth 268, 449-456 (2004).

[75] Y.-C. Hsu, Y.-K. Lin, M.-H. Chen, C.-C. Tsai, J.-H. Kuang, S.-B. Huang, H.-L. Hu, Y.-I Su, and W.-H. Cheng, "Failure Mechanisms Associated With Lens Shape of High-Power LED Modules in Aging Test," IEEE T. Electron. Dev. 55, 689-694 (2008).

[76] F.-K. Wang, and T.-P. Chu, "Lifetime predictions of LED-based light bars by accelerated degradation test," Microelectron. Reliab. 52, 1332-1336 (2012).

[77] S. I. Chan, W. S. Hong, K. T. Kim, Y. G. Yoon, J. H. Han, and J. S. Jang, "Accelerated life test of high power white light emitting diodes based on package failure mechanisms," Microelectron. Reliab. 51, 1806-1809 (2011).

[78] M.-H. Chang, D. Das, P. V. Varde, and M. Pecht, "Light emitting diode reliability review," Microelectron. Reliab. 52, 762-782 (2012).

[79] J.-M. Kang, J.-W. Kim, J.-H. Choi, D.-H. Kim, and H.-K. Kwon, "Life-time estimation of high-power blue light-emitting diode chips," Microelectron. Reliab. 49, 1231-1235 (2009).

[80] Projecting Long Term Luminous Flux Maintenance of LED Lamps and Luminaires, Illuminating Engineering Society, TM-28-14, USA, 2014.

[81] S. Koh, C. yan, B. Sun, B. Li, X. Fan, G. Q. Zhang, "Product Level Accelerated Lifetime Test for Indoor LED Luminaires," 14th International Conference on Thermal, Mechanical and Multi-Physics Simulation and Experiments in Microelectronics and Microsystems (EuroSimE)," Poland (2013).

[82] S. Levada, M. Meneghini, G. Meneghesso, and E. Zanoni, "Analysis of DC Current Accelerated Life Tests of GaN LEDs Using a Weibull-Based Statistical Model," IEEE Trans. Device Mater. Rel. 5, 688-693 (2005).

[83] G. Meneghesso, M. Meneghini, and E. Zanoni, "Recent results on the degradation of white LEDs for lighting," J. Phys. D: Appl. Phys. 43, 354007 (2010).

[84] A. Chrisntensen, and S. Graham, "Themal effects in packaging high power light emitting diode arrays," Appl. Therm. Eng. 29, 364-371 (2009).

[85] S.-H. Yu, K.-S. Lee, and S.-J. Yook, "Optimum design of a radial heat sink under natural convection," Int. J. Heat Mass Transfer 54, 2499-2505 (2011).

[86] S. Buso, G. Spiazzi, M. Meneghini, and G. Meneghesso, "Performance Degradation of High-Brightness Light Emitting Diodes Under DC and Pulsed Bias," IEEE Trans. Device Mater. Rel. 8, 312-322 (2008).

[87] D. L. Barton, M. Osinski, P. Perlin, P. G. Eliseev, and J. Lee, "Degradation of Single-Quantum Well InGaN Green Light Emitting Diodes Under High Electrical Stress," Microelectron. Reliab. 39, 1219-1227 (1999).

[88] L. Annaniah and M. Devaraja, "Investigation on Thermal Resistance of Cracked AlInGaP Die Substrate and In-line Die Crack Testing Method," J. Laser Opt. Photonics 3, 1000132 (2016).

[89] X. P. Li, L. Chen, and M. Chen, "An Approach of LED Lamp System Lifetime Prediction," Proceedings of the 2011 IEEE ICQR, 110-114 (2011).

[90] Y. P. Varshni, "Temperature dependence of the band gap in semiconductors," Physica 34, 149-154 (1967)

[91] A. Keppens, W. R. Ryckaert, G. Deconick, and P. Hanselaer, "High power light-emitting diode junction temperature determination from current voltage characteristics," J. Appl. Phys. 104, 093104 (2008).

[92] S. Suihkonen, T. Lang, O. Svensk, J. Sormunen, P. T. Törmä, M. Sopanen, H. Lipsanen, M. A. Odnoblyudov, and V. E. Bougrov, " Control of the morphology of InGaN/GaN quantum wells grown by metalorganic chemical vapor deposition," J. Cryst. Growth 300, 324-329 (2007).

[93] J. S. Blakemore, "Semiconducting and other major properties of gallium arsenide," J. Appl. Phys. 53, R213-R181 (1982).

[94] G. R. Moriarty, M. Kildemo, J. T. Beechinor, M. Murtagh, P. V. Kelly, G. M. Crean, and S. W. Bland, "Optical and structural properties of InGaP heterostructures," Thin Solid Films 368, 244-248 (2000).

[95] M. Zachau and W. T. Masselink, "Luminescence and Raman measurement of $In_yGa_{1-y}P$ (0.3<y<0.5) grown by gas-source molecular beam epitaxy," Appl. Phys. Lett 60, 2098 (1992).

[96] Y. Ishitani, S. Minagawa, and T. Tanaka, "Temperature dependence of the band-gap energy of disordered GaInP," J. Appl. Phys. 75, 5326-5331 (1994).

BUSINESS +
ECONOMY

ART +
DESIGN +
ARCHITECTURE

SCIENCE +
TECHNOLOGY

CROSSOVER

DOCTORAL
DISSERTATIONS